
**Separation Science and Technology**
Publication details, including instructions for authors and subscription information:
http://www.informaworld.com/smpp/title~content=t713708471

# Particle Trajectories in Field-Flow Fractionation and SPLITT Fractionation Channels

P. Stephen Williams[a]
[a] FIELD-FLOW FRACTIONATION RESEARCH CENTER DEPARTMENT OF CHEMISTRY, UNIVERSITY OF UTAH SALT LAKE CITY, UTAH

**To cite this Article** Williams, P. Stephen(1994) 'Particle Trajectories in Field-Flow Fractionation and SPLITT Fractionation Channels', Separation Science and Technology, 29: 1, 11 — 45
**To link to this Article: DOI:** 10.1080/01496399408002468
**URL:** http://dx.doi.org/10.1080/01496399408002468

SEPARATION SCIENCE AND TECHNOLOGY, **29**(1), pp. 11–45, 1994

# Particle Trajectories in Field-Flow Fractionation and SPLITT Fractionation Channels

P. STEPHEN WILLIAMS
FIELD-FLOW FRACTIONATION RESEARCH CENTER
DEPARTMENT OF CHEMISTRY
UNIVERSITY OF UTAH
SALT LAKE CITY, UTAH 84112



## ABSTRACT

The need for particle trajectory determination within field-flow fractionation and SPLITT fractionation channels is discussed. In the case of steric or steric/hyperlayer FFF, the trajectory followed by a particle determines its elution time. With hydrodynamic relaxation, the determination of a representative set of trajectories can also provide information on the band spreading inherent to the technique. In the simplest case of SPLITT fractionation where a binary separation is the objective, the trajectories determine the point at which a separative cut is made, as well as the sharpness of the cut. The influence of hydrodynamic lift forces, applied transverse and longitudinal fields, and secondary crossflow on particle migration are discussed, as well as the perturbing influence of the presence of the channel walls. Finally, a computer program is used to generate sets of particle trajectories to illustrate certain aspects of the preceding discussion.

## INTRODUCTION

The techniques of field-flow fractionation (FFF) and SPLITT fractionation (SF) are carried out within thin (generally submillimeter) channels of rectangular cross section of high aspect ratio (1–4). Both achieve separation of materials suspended or dissolved in a stream of carrier fluid flowing along the length of the channel. The rectangular cross section of the channel gives rise to a velocity profile for an isoviscous carrier that is parabolic across the thinner dimension and uniform across the breadth, except for small perturbations near the channel edges where the effect of drag at the side walls remains significant. These small edge perturbations are ignored

in the presence treatment. In both techniques the quality of separation is dependent on the flow velocity profile being constant across the channel breadth. This uniformity is contingent on the major walls being parallel. The high aspect ratio of the channels maximizes the permissible sample size while retaining the very short transport distances across the thickness that allow fast separations.

In this work we are concerned with the migration of particles that are not significantly influenced by Brownian effects. This is generally the case for particles larger in diameter than about 1 μm for typical channel dimensions and experimental time scales. Separation of such particles is achieved by the so-called steric (5–7) or steric-hyperlayer (8) modes of FFF. The normal mode of FFF (1, 4), whose mechanism is reliant on Brownian motion, will not be discussed here. The diffusion mode of operation for SPLITT systems (9, 10) will also not be considered.



Steric FFF, in common with all other modes of FFF, is a batch mode separation technique where material is separated due to differing migration velocity along the channel axis. To maximize separation it is therefore important that the initial sample band is narrow and that nonselective band spreading processes be minimized. The particulate sample is generally introduced to the channel as a narrow plug using a sample valve or syringe. The sample particles are driven toward one of the parallel walls (the accumulation wall) through interaction with a field applied across the channel thickness. In a flowing system the particle motion toward the accumulation wall is opposed by hydrodynamic forces which tend to increase with approach of the particle to the wall. It is often apparent that at some position above the wall the forces on a particle balance and an equilibrium point is established (6–8). For a particle separation to be realized in steric FFF, differing particles must be driven toward different equilibrium points above the accumulation wall. Their different equilibrium points within the parabolic velocity profile results in their different longitudinal migration velocities. To minimize nonselective band spreading it is essential that particles, identical in terms of the system selectivity, migrate toward their common equilibrium position in a time that is small compared to their elution time. If this is not achieved then particles which are initially distributed as a narrow band across the full channel thickness will be swept along the channel as they approach equilibrium. The initially narrow band would be spread out as those particles which are driven through the faster streamlines migrate further down the channel than those starting close to the accumulation wall (11, 12).

Two principal methods of reducing the band spreading incurred by slow migration toward equilibrium have been shown to be effective: stopped-

flow relaxation (12–14) and hydrodynamic relaxation (15–18). In the first, the sample is carried onto the channel at the normal channel flow rate, or at a reduced rate to aid in placing the sample reproducibly close to the channel inlet. The channel flow is then stopped, usually by valve switching to by-pass the channel, for a period sufficient for all sample components to be driven under the influence of the field into close proximity with the accumulation wall. The channel flow is subsequently reinstated. Particles then proceed to migrate toward their respective equilibrium positions from their starting points close to the wall. Provided there is no interference between particles, those that are identical will migrate coherently though the full length of the channel, even when the time for approach to equilibrium is not insignificant compared to elution time. The benefits of this approach are realized even when the time for migration to equilibrium is not small in comparison to the elution time. This relaxation time will generally be greatly reduced in any case because the distance from the accumulation wall to an equilibrium position is typically a small fraction of the channel thickness. Although this method is usually quite successful, it can result in loss of sample through adsorption on the channel wall during the primary stopped-flow relaxation period. The interruption in channel flow can also give rise to pressure pulses upon flow resumption and instability in baseline detector signal.



Hydrodynamic relaxation is achieved by the introduction of the sample into a generally small fraction of the channel flow. This fraction of the flow is confined hydrodynamically within a thin lamina adjacent to the accumulation wall by introducing the remaining fraction adjacent to the opposite (depletion) wall. This may be accomplished using either a split (15, 16) or frit (17, 18) inlet system. The split inlet has a thin plane splitter that extends a short distance into the channel. It is mounted parallel to the major walls and divides two inlet ports that enter at each side of the channel. The generally slower flow into which the sample is introduced enters at the accumulation wall and the remainder is made up at the other inlet. Under conditions of laminar flow the sample is initially confined below a stream plane that extends from the splitter edge through the length of the channel. The thickness of the sample lamina may be adjusted via the inlet flow rate ratio, as explained later. The frit inlet has a small region of the depletion wall at the channel inlet that is composed of a permeable frit material. The generally larger portion of the channel flow that is used to hydrodynamically drive the sample toward the accumulation wall is introduced via the frit. Again, the sample lamina thickness may be adjusted via the ratio of the flow rate at the frit to the initial channel flow rate. With hydrodynamic relaxation particles have a much reduced migration

distance toward their respective equilibrium positions, and nonselective band spreading is consequently reduced. The process is achieved without interruption of flow and therefore with less chance of adsorption on the channel wall.

Unlike the FFF techniques, SPLITT fractionation (SF) does not depend on the different elution times of sample components (2, 19). The separation of materials across the cell thickness is exploited. This separation is obtained as sample components migrate toward different equilibrium positions, or as sample components migrate at different rates toward either the same or different equilibrium positions. The former situation is exploited by the equilibrium mode of SF, and the latter by the transport mode. For the transport mode of operation it is essential that the sample be initially confined to a narrow region of the cell thickness, and this is achieved using an inlet splitter. For the equilibrium mode an inlet splitter is not necessary, provided sufficient time is allowed for sample migration. In either mode the separated components are directed to different cell outlets by use of one or more flow splitters. As in the case of the inlet splitter described for hydrodynamic relaxation in FFF, the positions of the outlet splitting planes (OSPs) may be adjusted via the relative outlet volumetric flow rates.

A binary separation is achieved with the use of a single outlet splitter, and for practical reasons this is generally how SPLITT cells are constructed and operated. The use of two or more flow splitters at the outlet to obtain higher order separations has been discussed (2). Construction of these systems would be more complicated. The resolution of components would be compromised by any imperfection in a splitter such as a burred edge, curvature, or deviation from parallel placement with neighboring splitters or cell walls. The chance of imperfection would increase with the number of splitters in the system. Higher order separations may more easily be obtained using series coupled binary SPLITT systems (2, 20). As mentioned earlier, SPLITT fractionations do not depend on differential elution times. Components are simply recovered at different outlets. A conventional SPLITT cell may be capable of only a binary separation, but its strength lies in its capacity for continuous mode fractionation. Such operation is referred to as continuous SPLITT fractionation (CSF).

The flow of carrier fluid in SPLITT cells, just as in FFF channels, leads to the generation of hydrodynamic forces on entrained particles. These forces alone may be utilized to obtain SPLITT cell fractionations (21, 22). However, it is common practice to apply an external field across the cell thickness to induce transverse migration in the same manner as in FFF. The field types used for FFF are equally applicable to SF. In the case

of FFF these have included gravitation (23), centrifugation (16), thermal gradient (11, 24, 25), and electrical (26). Gravitational (20, 27), centrifugal (28), and electrical (29) fields have been used successfully for SF to date. In addition to those fields mentioned above, the use of a secondary cross flow through semipermeable channel walls has been employed in both FFF (8, 30, 31) and SF (3, 32). As we shall see below, there is a fundamental difference in predicted particle motion within a cross flow as opposed to motion under the influence of an applied field. Within a cross flow a particle is simply displaced with the transverse velocity of the surrounding fluid. Motion induced by an applied field drives the particle through the surrounding fluid. The field-induced velocity of the particle toward, or away from, a wall bounding the fluid is influenced by the presence of the wall. The effective particle friction coefficient increases, and its velocity decreases, with approach to a wall because fluid has to be continuously removed from the closing gap.



In our treatment of particle trajectories we shall consider the influence of hydrodynamic lift forces, an applied transverse field, a secondary cross flow, or any combination of these. In addition, since SPLITT cells are sometimes operated in a vertical orientation to reduce the effects of gravity on transverse migration, the influence of field-induced migration along the axis of flow is considered. This migration contributes to the overall particle velocity along the cell at any given transverse position. In addition, field-induced axial migration has a strong influence on hydrodynamic lift forces. Both effects are taken into account. Our treatment is therefore applicable to any orientation of SPLITT cell from vertical with upward flow, through horizontal, to vertical with downward flow. We do not consider migration across the breadth of these systems. In practice, such migration should generally be avoided so that material is not driven into the regions of perturbed flow velocity near the channel edges. This is achieved by ensuring that no field that interacts with the sample material has a cross-channel component.

Trajectories have previously been determined for neutrally buoyant particles entrained in plane Poiseuille flow between impermeable walls (33), between an impermeable and a permeable wall (with outflow) (34–37), and between two permeable walls (with outflow at both) (38). These treatments did not, however, take into account the perturbing influence of the walls on particle motions. The influence of applied fields in transverse and longitudinal directions was also not considered. Transverse fields are an essential element of FFF and of most applications of SF. Our approach to trajectory determination takes into account all essential factors that govern particle separations within FFF channels and SPLITT cells.

## THEORY

### FFF Channel and SPLITT Cell Conventions

Edge views of the two systems are shown in Fig. 1. They are not drawn to scale since the length to thickness ratio for SPLITT cells is typically between 50 and 500, whereas for FFF channels this ratio typically falls between 1000 and 10,000. The difference is mainly due to differences in length, SPLITT cells being typically between 2 and 20 cm long and FFF channels between 20 and 100 cm. The simpler construction of conventional FFF channels (i.e., those without flow splitters) also allows them to be made thinner than the sandwich-constructed SPLITT cells.

In each case the system has a thickness $w$, breadth $\bar{b}$, length $L$, and void volume $V^0$ ($=L\bar{b}w$). For FFF channels the length is measured either from the edge of the inlet splitter or from the point of primary relaxation, depending on the type of relaxation used, to the channel outlet. For SPLITT cells the length is measured between the splitters. The $x$ coordinate extends across the thickness and has its origin at the accumulation wall for FFF channels, and at wall A adjacent to sample input for SPLITT



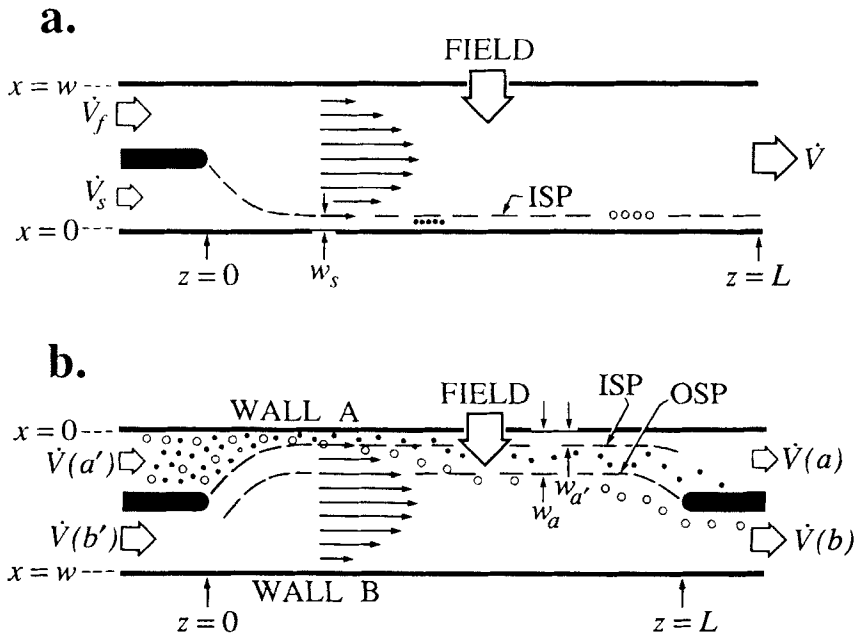


FIG. 1 Edge views of (a) FFF channel with split inlet and (b) SPLITT cell operated in transport mode.

cells. The $z$ coordinate extends along the system length in the direction of flow. Total channel flow $\dot{V}$ through the system is made up of sample flow $\dot{V}_s$ and supplementary flow $\dot{V}_f$ for frit or split inlet FFF, and of sample flow $\dot{V}(a')$ and supplementary carrier flow $\dot{V}(b')$ for SF. For the latter, the flow is divided into $\dot{V}(a)$ and $\dot{V}(b)$ at the outlet splitter, the flows exiting adjacent to walls A and B, respectively. The mean fluid velocity through the system $\langle v \rangle$ is given by $\dot{V}/\bar{b}w$, and the parabolic velocity profile across the channel thickness, ignoring side wall effects, by

$$v\left(\frac{x}{w}\right) = 6\langle v\rangle \frac{x}{w}\left(1 - \frac{x}{w}\right) = 4v_{max}\frac{x}{w}\left(1 - \frac{x}{w}\right) \tag{1}$$

where $v_{max}$ is the maximum velocity found at the channel midpoint and is equal to $(3/2)\langle v \rangle$. Consideration of this parabolic velocity profile shows that the distance $w_{a'}$ from wall A to the inlet splitting plane (ISP) is given by (9)

$$w_{a'}/w = \sin(\theta/3) + 0.5 \tag{2}$$

where

$$\sin(\theta) = 2\frac{\dot{V}(a')}{\dot{V}} - 1 \tag{3}$$

and $-\pi/2 < \theta \leq \pi/2$. The ratio of $\dot{V}(a)/\dot{V}$ required to place the outlet splitting plane (OSP) at a distance $w_a$ from wall A is given by (9, 21)

$$\frac{\dot{V}(a)}{\dot{V}} = 3\left(\frac{w_a}{w}\right)^2 - 2\left(\frac{w_a}{w}\right)^3 \tag{4}$$

The sign convention for all fields together with resultant forces on particles, and cross flow if present, follows the $x$ and $z$ coordinate convention. The primary field in FFF therefore has a negative sense, whereas the optional field in SF acts in a positive direction. Vertical orientation of a SPLITT cell with downward flow experiences a positive gravitational field. For upward flow, where the $z$ coordinate is reversed, gravity acts in the negative direction.

## Hydrodynamic Lift Forces

Cox and Brenner (39) derived expressions describing the force required to prevent the transverse migration, due to fluid inertial effects, of a particle of arbitrary shape entrained in bounded, low Reynolds number flows. The expressions were later solved for the special case of a spherical particle in plane Poiseuille flow (33, 40, 41). The transverse force $F_{Li}(I)$ on a

neutrally buoyant particle entrained in such a bounded flow (we include the subscript $i$ to indicate that it is due to inertial effects, and the numerical $I$ to distinguish this from the the other inertial contributions described by Eqs. 11 and 13) was found to be given by (33, 40)

$$F_{Li}(I) = 6\pi \frac{v_{max}^2 a^4 \rho}{w^2} g\left(\frac{x}{w}\right) \tag{5}$$

where $a$ is the particle radius, $\rho$ is the fluid density, and $g(x/w)$ is given approximately by

$$g\left(\frac{x}{w}\right) \approx \frac{55}{36}\left(1 - \frac{x/w}{0.19}\right)\left(1 - \frac{x/w}{0.5}\right)\left(1 - \frac{x/w}{0.81}\right) \tag{6}$$

so that

$$g\left(\frac{x}{w}\right) \approx 19.85\left(0.19 - \frac{x}{w}\right)\left(0.5 - \frac{x}{w}\right)\left(0.81 - \frac{x}{w}\right) \tag{7}$$

The initial quotient on the right-hand side of Eq. (6) is consistent with the limiting magnitude of the lift force predicted by Cox and Hsu (41) for flow bounded by a single wall. The cubic in $x/w$ is also consistent with the predicted zeros of the lift force function. A sixth-order polynomial approximation of Otis (42), reported by Belfort and Nagata (36), indicates that our cubic equation increasingly underestimates the magnitude of the lift force toward the channel center. The symmetry of the lift force indicates that a polynomial fit should be of an odd order. We propose the following improved approximate polynomial expression of fifth order for $g(x/w)$:

$$g\left(\frac{x}{w}\right) \approx 19.85\left(0.19 - \frac{x}{w}\right)\left(0.5 - \frac{x}{w}\right)\left(0.81 - \frac{x}{w}\right)\left[1 + \frac{16}{25}\frac{x}{w}\left(1 - \frac{x}{w}\right)\right] \tag{8}$$

This results in the correct limiting lift force near the walls [as predicted by Cox and Hsu (41)], and a force magnitude in the central regions consistent with the sixth-order polynomial approximation reported by Belfort and Nagata (36).

The derivation of Eq. (5) requires that $a/w$, $a/x$, and $a/(w - x)$ are all small compared to unity (i.e., the particles must be small compared to the channel thickness, and must not be close to either wall). The channel Reynolds number Re ($= w v_{max}\, \rho/\eta$, where $\eta$ is the fluid viscosity) was also required to be small compared to unity, but Schonberg and Hinch (43) have since shown that this condition may be relaxed considerably. The inertial force described by Eqs. (5) and (8) tends to drive particles

away from the walls and also away from the channel center line. Under conditions where no other forces act upon the particles, they would be driven toward two equally stable equilibrium positions at $x/w = 0.19$ and 0.81. An unstable equilibrium point is located at the channel center line.

The magnitude of these predicted forces is very weak. For example, the force exerted on a neutrally-buoyant 10 μm particle, with its center 20 μm from a wall, with an aqueous carrier flowing at $\langle v \rangle = 10$ cm/s within a 330-μm channel, would be only $2.13 \times 10^{-7}$ dynes. According to Stokes' law, this would nevertheless result in a transverse velocity of 25.4 μm/s (assuming $\eta = 0.0089$ poise). If the particle center was 40 μm from the wall, the force would fall to $9.26 \times 10^{-8}$ dynes and the velocity to 11.0 μm/s. These velocities are small but significant when compared to the very small transport distances typical of SPLITT cells.

For a vertically oriented channel the criterion for neutral buoyancy of the entrained particles may be written as

$$| U_z | \ll \left(\frac{a}{w}\right)^2 v_{max} \tag{9}$$

where $U_z$ is the sedimentation velocity of the particle in unbounded fluid (i.e., the Stokes' velocity). If there is a density difference between particles and fluid there will be a tendency for them to be driven gravitationally either ahead of or against the flow. The effect of such motion on the predicted inertial force has been considered by Vasseur and Cox (40) and by Cox and Hsu (41). It results in an additional contribution to lift, which for small $x/w$ is approximated by the single wall solution derived by Cox and Hsu (41). This may be written in the form

$$F_{Li}(II) = -\frac{315}{16} \pi U_z v_{max} a^2 \rho \frac{x}{w}\left(\frac{22}{105} - \frac{x}{w}\right) \tag{10}$$

which is in agreement with the two-wall solution (40) only for $x/w < 0.1$. The limiting behavior at the opposite wall is given by replacing $x/w$ with $(1 - x/w)$ and removing the leading negative sign. The behavior within the region $0.1 < x/w < 0.9$ is not well described by Eq. (10). The two-wall solution (40) shows that the magnitude of this lift contribution is zero at the walls, increases to maxima at $x/w$ close to 0.19 and 0.81, and falls to zero at $x/w = 0.5$. We propose that the lift due to the two walls may be approximated by the following simple fifth-order polynomial expression:

$$F_{Li}(II) \approx -\frac{33}{4} \pi U_z v_{max} a^2 \rho \frac{x}{w}\left(0.5 - \frac{x}{w}\right)\left(1 - \frac{x}{w}\right)\left[1 - \frac{5}{2}\frac{x}{w}\left(1 - \frac{x}{w}\right)\right] \tag{11}$$

The agreement with the solution presented by Vasseur and Cox (40) is greatly improved by the inclusion of the final quadratic factor.

From Eq. (11) we see that if the particles sediment against the flow, the additional contribution tends to drive them away from the walls. The result is that the equilibrium positions approach the channel center as $(-U_z/v_{max})(w/a)^2$ increases (i.e., as the contribution of Eq. 11 increases relative to that of Eq. 5). When $(-U_z/v_{max})(w/a)^2 \approx 15$, the equilibrium positions converge on the channel center line. An example is shown in Fig. 2(a), which represents the situation of a 10-μm diameter silica particle entrained in upward aqueous flow in a 330-μm thick cell. The sedimentation velocity $U_z$ is calculated to be $-0.0092$ cm/s, assuming the excess density of the particle over that of the fluid $\Delta\rho = 1.5$ g/mL. This small downward sedimentation velocity in an upward flow for which $v_{max} = 2.67$ cm/s is sufficient to effectively merge the equilibrium positions at the channel center.

The situation is more complicated for particles that sediment in the direction of flow. The additional contribution of Eq. (11) in this case acts toward the walls. Consequently, the equilibrium positions at first approach the walls with increase of $U_z$ (i.e., as the condition given by Eq. 9 is violated to a greater and greater extent). Figure 2(b) shows the result of reversing the direction of flow for the example considered in Fig. 2(a). Our approximate expressions predict that the equilibrium positions are moved toward the walls, to $x/w$ close to 0.1 and 0.9. Vasseur and Cox (40) predicted that when $U_z > \sim 20(a/w)^2 v_{max}$ the equilibrium points will be found at $x/w < 0.1$ and $x/w > 0.9$; further increase of $U_z$ brings the equilibrium points even closer to the walls. However, when the sedimentation velocity $U_z$ becomes of the same order of magnitude as $v_{max}$, there is a reversal in this trend as yet another force contribution that acts away from the walls becomes increasingly significant. This contribution also has a fluid inertial origin. The sedimentation of a spherical particle through a quiescent fluid parallel to a vertical bounding wall results in a force on the particle in the direction away from the wall (44). The force is given by

$$F_{Li}(III) = \frac{9}{16}\pi U_z^2 a^2 \rho \tag{12}$$

provided $xU_z\rho/\eta \ll 1$. We propose the following fifth-order polynomial to describe the sum of the contributions due to the opposing walls of a parallel plate system:

$$F_{Li}(III) \approx \frac{9}{8}\pi U_z^2 a^2 \rho \left[1 + \frac{x}{w} - \left(\frac{x}{w}\right)^2\right]^2 \left(0.5 - \frac{x}{w}\right) \tag{13}$$

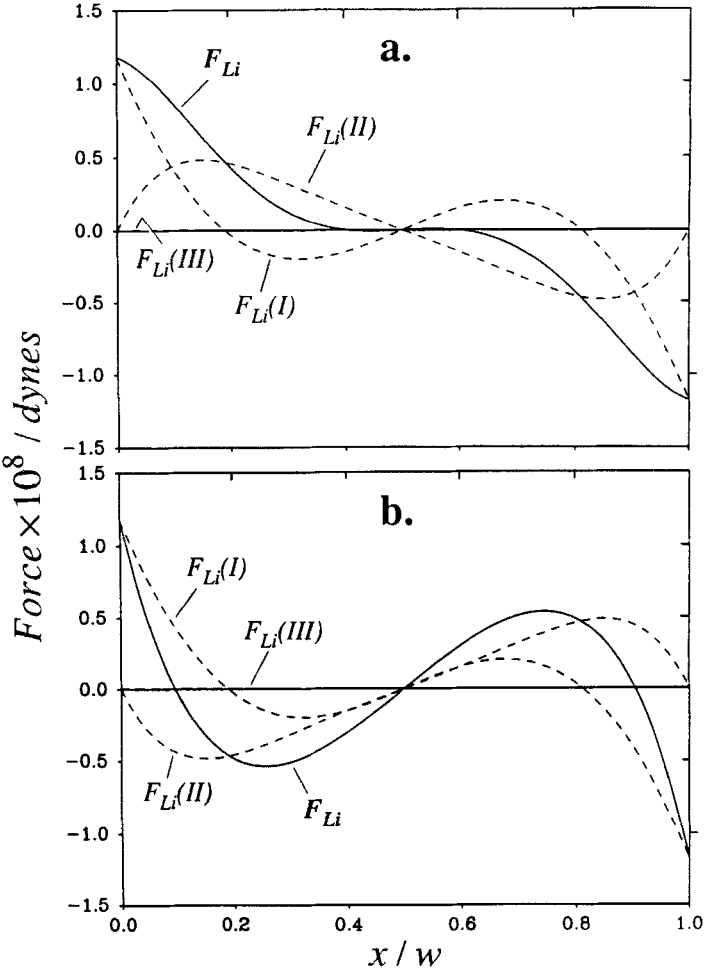


FIG. 2 Plots of the contributions $F_{Li}(I)$ (described by Eqs. 5 and 8), $F_{Li}(II)$ (described by Eq. 11), $F_{Li}(III)$ (described by Eq. 13), and the resultant total inertial lift force $F_{Li}$ for a 10-μm silica particle entrained in aqueous flow in a 330-μm thick channel with $v_{max}$ = 2.67 cm/s: (a) upward flow and (b) downward flow. Contribution $F_{Li}(III)$ is negligible under these conditions.

which has a limiting slope of zero at the walls and quite closely follows the true variation, as described by Vasseur and Cox (40), across the channel thickness.

When $U_z$ and $v_{max}$ are of the same order of magnitude, the contributions to lift described by Eqs. (11) and (13) dominate. Equilibrium points correspond once again to $x/w = 0.1$ and 0.9 when $U_z/v_{max} \approx 0.39$, and then rapidly approach $x/w = 0.5$ at $U_z/v_{max} = 0.5$ (see Ref. 40). When sedimentation is in the opposite direction to flow, the two contributions in concert act to drive particles toward the channel center. An example of the latter situation is shown in Fig. 3(a). The figure shows the result for a 20-μm copper particle entrained in upward aqueous flow within a 330-μm cell. The sedimentation velocity $U_z$ is calculated to be $-0.19$ cm/s, taking $\Delta\rho = 7.92$ g/mL, and the upward flow is considered to correspond to $v_{max} = 0.38$ cm/s. The situation corresponding to reversed flow is shown in Fig. 3(b). The equilibrium positions are seen to be extremely sensitive to small variations in the ratio of $U_z/v_{max}$ around the critical value of 0.5. The figure shows that at the critical ratio the force away from the walls is maintained, but inertial lift force is effectively neutralized across a large central portion of the channel thickness.

In summary, it was shown that when $(-U_z/v_{max})(w/a)^2 > 15$ or when $U_z/v_{max} > 0.5$, particles are predicted to migrate toward the channel center. Intermediate conditions result in two stable equilibrium positions on opposing sides of the channel.

As mentioned above, inertial lift forces are not well described for regions close to the bounding walls. Steric field-flow fractionation has provided an experimental means of studying near-wall hydrodynamic lift force (45). Steric field-flow fractionation is an analytical elution technique that separates particles principally on the basis of size (see, for example, Ref. 6). The separation is carried out within a thin parallel-walled channel of similar cross section to typical SPLITT cells. The particles are driven toward one of the walls by an applied field such as centrifugation. The forces on the various particle sizes are, at different points, exactly balanced by opposing lift forces. The different equilibrium points for the different particle sizes result in their different elution velocities within the parabolic flow profile. Systematic studies using various particle sizes, field strengths, flow rates (45), and recently carrier viscosities (46) have shown that in the near-wall region the lift force is described by the empirical equation

$$F_{Lw} = C\frac{a^3\eta s_0}{\delta} = \frac{6Ca^3\eta\langle v\rangle}{w\delta} = \frac{4Ca^3\eta v_{max}}{w\delta} \tag{14}$$

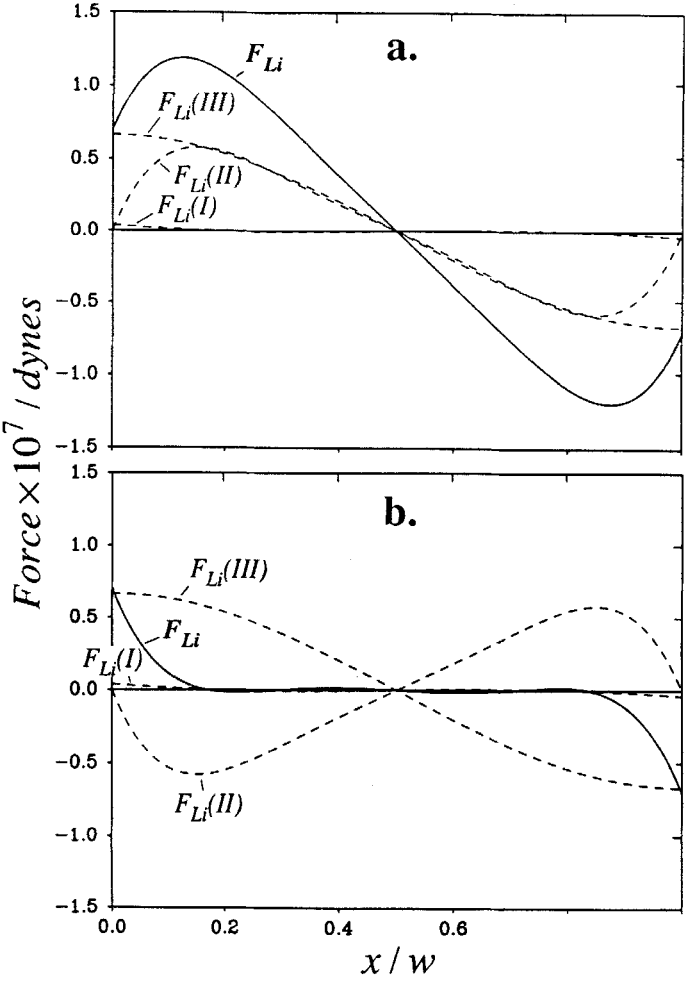


FIG. 3 Plots of the contributions $F_{Li}(I)$ (described by Eqs. 5 and 8), $F_{Li}(II)$ (described by Eq. 11), $F_{Li}(III)$ (described by Eq. 13), and the resultant total inertial lift force $F_{Li}$ for a 20-μm copper particle entrained in aqueous flow in a 330-μm thick channel with $v_{max}$ = 0.38 cm/s: (a) upward flow and (b) downward flow.

where $C$ is a dimensionless coefficient that has some system dependence that is not yet fully characterized, $s_0$ is the undisturbed carrier shear rate at the wall, and $\delta$ is the distance between the particle surface and the wall and is equal to $(x - a)$. Close to the wall $F_{Lw}$ is apparently inversely proportional to $\delta$, for the range of $\delta$ studied, and far exceeds the lift force predicted for inertial effects. On the other hand, the lift predicted by Eq. (14) is very quickly attenuated for particles removed from the vicinity of the wall. It has been found (47) that hydrodynamic lift from a wall bounding plane Poiseuille flow is consequently quite well described as a simple sum of the contributions of Eqs. (5) and (14) when no net force operates in the direction of flow. We may account for near-wall lift in a parallel plate system by summing the contributions due to each wall as follows:

$$F_{Lw} = \frac{6Ca^3\eta\langle v\rangle}{w}\left(\frac{1}{(x-a)} - \frac{1}{(w-x-a)}\right) \tag{15}$$

The near-wall lift contribution will tend to drive particles a little beyond the points where inertial effects have a zero net influence (at $x/w = 0.19$ and 0.81 for neutrally buoyant particles). The equilibrium points will therefore lie within, but generally close to, $x/w = 0.19$ and 0.81. Of course, if particles are large enough to be sterically excluded from the inertial equilibrium points, then the near-wall contributions are likely to dominate throughout the channel. For such a case a single central equilibrium point would result. For intermediate sizes, a particle size effect on the equilibrium points would therefore be expected.

It must be pointed out that, to date, the near-wall lift force on a particle sedimenting through a quiescent fluid, in close proximity to a bounding wall, has not been studied experimentally. It is unknown if the particle would be acted upon by an enhanced lift force, relative to that described by Eq. (13).

## Forces Due to Interaction with Transverse Applied Field

The force on a spherical particle due to a transverse gravitational or centrifugal field is given by

$$F_x = \frac{4}{3}\pi a^3 \Delta\rho G_x \tag{16}$$

where $\Delta\rho$ is the difference in density between the particle and the fluid $(=\rho_s - \rho$, where $\rho_s$ is the particle density), and $G_x$ is the transverse field

strength (acceleration). A thermal gradient generates a force described by (24, 25)

$$F_x = 6\pi\eta a D_T \frac{dT}{dx} \tag{17}$$

where $D_T$ is the thermal diffusion coefficient of the particle in the solvent, and $dT/dx$ is the temperature gradient. A transverse electrical field generates a force described by

$$F_x = ze \frac{dV}{dx} \tag{18}$$

where $z$ is the effective charge number on the particle, $e$ is the charge on the electron, and $dV/dx$ is the voltage gradient. Transverse fields may be applied in combination, the net force on the particle then being the sum of the individual contributions.



## Field and Lift-Induced Migration of Particles Perpendicular to Walls

Motion of a particle through a viscous fluid toward or away from a plane wall is perturbed by disturbance flows generated by the changing gap width between the particle and the wall. To account for this perturbation Maude (48) and Brenner (49) derived an expression for a correction factor $\Gamma_{1x}$ to the particle friction factor. The subscript $x$ is included here to indicate that the correction is applicable to motion parallel to the $x$-axis (i.e., perpendicular to the wall), and the subscript 1 to indicate that the correction refers to migration perpendicular to a single wall. The expression involves the sum of an infinite series of terms in hyperbolic functions and is given by

$$\Gamma_{1x} = \frac{4}{3} \sinh \alpha \sum_{n=1}^{\infty} \frac{n(n+1)}{(2n-1)(2n+3)} \times \left[ \frac{2 \sinh(2n+1)\alpha + (2n+1) \sinh 2\alpha}{4 \sinh^2(n+0.5)\alpha - (2n+1)^2 \sinh^2 \alpha} - 1 \right] \tag{19}$$

where

$$\alpha = \cosh^{-1}\left(\frac{x}{a}\right) = \ln\left\{\frac{x}{a} + \left[\left(\frac{x}{a}\right)^2 - 1\right]^{0.5}\right\} \tag{20}$$

The correction factor $\Gamma_{1x}$ is therefore a function of only the ratio $x/a$, or equivalently, of $\delta/a$. The value of $\Gamma_{1x}$ approaches infinity as the gap between the particle and the wall approaches zero, although in practice surface roughness and/or cavitation is expected to limit the range of applicability of the equations (49). From high values close to the wall the correction factor falls monotonically to unity as the particle is removed from the wall.

The derivation of the expression for $\Gamma_{1x}$ does not take into account any inertial effects and requires particle Reynolds number $av_{px}\rho/\eta$ to be small compared to unity. Conditions of quasi-steady flow were also assumed, so that the time-dependent term of the Navier–Stokes equation could be ignored. This assumption requires that $a^2v_{px}\rho/\eta\delta$ be small. Cox and Brenner (50) have since obtained a first-order correction for inertial effects at small gap widths, but we shall not concern ourselves here with this relatively small effect. We note also that Durst and Raszillier (51) presented a more refined theoretical treatment which shows that $\Gamma_{1x}$ tends to overcorrect the friction factor. The derivation of $\Gamma_{1x}$ assumes local equilibrium between the driving force and the opposing drag force, and this assumption becomes increasingly in error as the ratio of the product of Stokes' velocity and relaxation time (i.e., the time to attain this velocity from rest) to the particle radius increases. The error therefore increases for larger and/or denser particles at high field strengths. We shall not consider this refinement in our trajectory calculations but recognize that some error will be incurred under extreme conditions.



Experimental observations of particles settling under gravity (52–54) and direct measurement of the drag force on particles moving at constant $v_{px}$ (55) proved to be in excellent agreement with predicted $\Gamma_{1x}$ for $\delta/a$ as low as 0.01.

When the particle is close to the wall (i.e., $\delta/a \ll 1$), the full expression of Maude and Brenner reduces to (53, 56)

$$\Gamma_{1x} = \frac{a}{\delta} = \frac{a}{x - a} \tag{21}$$

which is good only for very small $\delta/a$. Cox and Brenner (50) derived an improved approximation for $\Gamma_{1x}$, valid for $\delta/a \ll 1$, given by

$$\Gamma_{1x} = \frac{a}{\delta} + \frac{1}{5}\ln\left(\frac{a}{\delta}\right) + 0.971264 \tag{22}$$

Cooley and O'Neill (57) obtained essentially the same result, differing only in the fifth decimal place of the constant (they obtained a value of 0.971280).

When the particle is far from the wall (i.e., $x/a \gg 1$), the full expression for $\Gamma_{1x}$ reduces to (48)

$$\Gamma_{1x} = 1 + \frac{9}{8}\left(\frac{a}{x}\right) \tag{23}$$

which agrees with the result obtained by Lorentz (58) for this situation.

Figure 4 shows a plot of the function $\Gamma_{1x}$ (calculated using the full expression) versus $\log_{10}(\delta/a)$. Plots of the limiting expressions for small and large $\delta/a$, given by Eqs. (22) and (23), respectively, are also included. The percentage deviation of these limiting expressions from $\Gamma_{1x}$ are shown above the main figure. Equation (22) underestimates $\Gamma_{1x}$ by 1.0% at $\delta/a = 0.239$, by 0.10% at $\delta/a = 0.0605$, and by 0.010% at $\delta/a = 0.0166$. The less accurate expression of Eq. (21) underestimates $\Gamma_{1x}$ by 1.0% even at $\delta/a = 0.00497$. At the other extreme Eq. (23) underestimates $\Gamma_{1x}$ by 1.0% at $\delta/a = 10.1$, by 0.10% at $\delta/a = 34.4$, and by 0.010% at $\delta/a = 111.0$. In practice, accurate values for $\Gamma_{1x}$ may be obtained using Eq. (22) for $\delta/a$



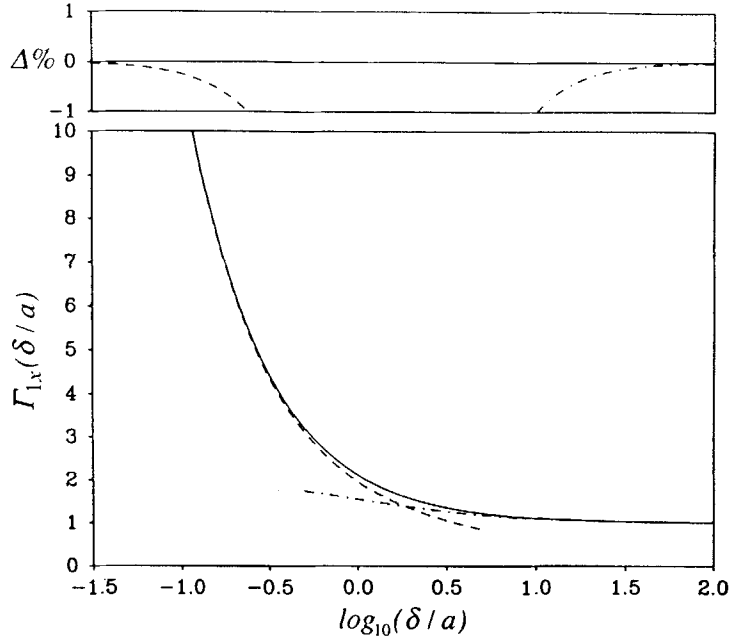


FIG. 4 Plot of the function $\Gamma_{1x}$ as described by Eq. (19), together with the limiting Eqs. (22) and (23). The percentage deviations of the latter equations from $\Gamma_{1x}$ are shown above the main figure.

$< 0.0166$, the full Maude–Brenner expression (Eq. 19) for $0.0166 \leq \delta/a < 111.0$, and Eq. (23) for $111.0 \leq \delta/a$. Only 18 terms of the Maude–Brenner expression require summation to achieve similar accuracy to Eq. (22) at $\delta/a = 0.0166$, and much fewer at larger $\delta/a$.

The correction to particle friction factor for the migration of a spherical particle across the thickness of a parallel-walled channel has been determined numerically by Ganatos, Weinbaum, and Pfeffer (59). Results for a few selected conditions were tabulated and graphed. As one might expect, the perturbation for a small particle (for which $a/w \ll 1$) located close to one of the walls is dominated by the presence of the nearer wall. In fact, the further wall exerts little influence up to $x/w = 0.3$, even for relatively large particles. For example, for a particle corresponding to $a/w = 0.1$ located at $x/w = 0.3$, $\Gamma_{1x}$ is only ~3% lower than the two-wall correction factor $\Gamma_x$ (i.e., the nearer wall accounts for 97% of $\Gamma_x$). For the same size particle at $x/w = 0.2$, $\Gamma_{1x}$ is just 2% lower than $\Gamma_x$. Smaller errors are given for smaller particles. If migration across the full thickness is of interest, then a good estimate for the overall correction factor $\Gamma_x$ may be made via a first-order approximation given by

$$\Gamma_x\left(\frac{x}{a}, \frac{w - x}{a}\right) = \Gamma_{1x}\left(\frac{x}{a}\right) + \Gamma_{1x}\left(\frac{w - x}{a}\right) - 1 \tag{24}$$

This expression tends to overestimate $\Gamma_x$ to a small extent, particularly toward the channel center where the two walls provide similar contributions to the perturbation. For example, $\Gamma_x$ for the relatively large particle corresponding to $a/w = 0.1$ is overestimated by 12% at $x/w = 0.5$, 9% at $x/w = 0.3$, and 5% at $x/w = 0.2$. Once again, errors are reduced for smaller particles.

The instantaneous migration velocity component $v_{px}$ of a particle along the $x$ coordinate is then given by

$$v_{px} = \frac{F_L + F_x}{6\pi\eta a\Gamma_x} \tag{25}$$

where $F_L$ is the local strength of the lift force on the particle (given by the sum of the contributions described by Eqs. 5, 11, 13, and 15), $F_x$ is the net local force due to applied transverse fields, and $\Gamma_x$ is the local correction to particle friction factor, given by the Stokes–Einstein expression ($6\pi\eta a$) in the equation above. When a particle is in close proximity to a wall ($x$ is only just larger than $a$, for example), the lift force will be dominated by the near-wall component described by Eq. (14), and $\Gamma_x$ will be closely approximated by Eq. (21). The magnitude of $F_x$ approaches

insignificance as $F_L$ approaches infinity (see Eq. 14 with $\delta \rightarrow 0$), and the velocity $v_{px}$ is then given by

$$v_{px} = \frac{2Cav_{max}}{3\pi w} = \frac{Ca\langle v \rangle}{\pi w} \tag{26}$$

Proximity to the opposite wall would result in equal, but opposite, limiting velocity.

## Transverse Migration of Particles in Porous Walled Channels

The theory presented thus far is applicable strictly to systems with nonpermeable walls. We can expect increasing perturbation with an increase of wall permeability. The no-slip assumption for fluid at the surface of a porous wall cannot be made (60, 61). Inertial lift forces will be reduced near the walls since disturbance flows around the particle may enter the surface of the wall (35). The apparent near-wall lift force described by Eq. (15) may also be reduced. This reduction in lift forces will, however, be offset to a certain extent by a reduction in $\Gamma_x$. Such a reduction was predicted for the related case of the approach of a permeable sphere toward an impermeable wall (62). The lateral velocity is therefore likely to be perturbed to a lesser degree than either lift force or correction to particle friction factor.

In our treatment we shall assume negligible perturbation due to wall permeability, and a simple additivity of lift- and field-induced velocity and cross flow velocity. These assumptions were made by Belfort and coworkers (34–37, 63) and by Kleinstreuer and Chin (38). We assume that the channel walls are uniformly permeable and that the cross flow rate $\dot{V}_c$ that enters one wall is withdrawn at the opposite wall. The cross-flow velocity of the fluid is then uniform and given by $\dot{V}_c/L\bar{b}$. Hence, when a cross flow is considered, Eq. (25) becomes

$$v_{px} = \frac{F_L + F_x}{6\pi\eta a\Gamma_x} + \frac{\dot{V}_c}{L\bar{b}} \tag{27}$$

and, for regions close to the wall at which $x = 0$ (i.e., the accumulation wall in FFF, or wall A in SF), we obtain

$$v_{px} = \frac{Ca\langle v \rangle}{\pi w} + \frac{\dot{V}_c}{L\bar{b}} \tag{28}$$

Equation (28) suggests that if $\dot{V}_c$ is negative and sufficiently large, then $v_{px}$ can be negative, with the result that the particle would be driven into

contact with the wall and its migration along the channel halted. Similarly, if $\dot{V}_c$ is positive and sufficiently large, then the particle would be driven into the opposite wall. The equation may be rearranged to determine a critical particle radius that will elute through the system:

$$a_{crit} = \frac{\pi w \mid \dot{V}_c \mid}{C\langle v \rangle L\bar{b}} = \frac{\pi w^2}{CL} \frac{\mid \dot{V}_c \mid}{\dot{V}} \tag{29}$$

All particles smaller than this critical size are predicted to contact one or other of the walls. Equation (29) suggests, for example, that the critical particle size for elution in flow-hyperlayer FFF is dependent on the ratio of cross flow rate to channel flow rate.

## Migration of Particles Parallel to Walls

Goldman, Cox, and Brenner (64) showed how the velocity of a particle moving through a quiescent viscous fluid, parallel to a bounding wall, may be determined via consideration of the forces and torques exerted on the particle due to its translation and rotation. Inertial effects were not considered, and so the results are applicable to small particle Reynolds numbers only. They computed the relevant forces and torques for various $\delta/a \geq 0.0032$ via the earlier rigorous approach of Dean and O'Neill (65) and O'Neill (66), correcting the results of the former and confirming those of the latter. They also derived the limiting dependencies of the forces and torques on $\delta/a$ for $\delta/a \rightarrow 0$ using a lubrication theory approach. The limiting dependencies obtained via the two approaches were consistent. The zeroth-order terms obtained for the latter approach were not acceptable, however, due to slow computational convergence. These terms were corrected by matching with the results of the former approach. Limiting equations for small $\delta/a$ were thus obtained. Limiting equations for large $\delta/a$ were derived by Faxén (67), Maude (68), and Goldman et al. (64). Higher order limiting expressions for low gap widths have since been derived by O'Neill and Stewartson (69) and by Cooley and O'Neill (70).

For a particle acted upon by a force parallel to the wall, we may formulate the result in terms of a correction to the particle friction factor, as obtained for the case of migration perpendicular to the walls. Using the limiting equations reported by Goldman et al. (64) for small gap widths, we obtain

$$\Gamma_{1z} = \frac{1}{2}\left\{\frac{1.5905 - 3.1881 \ln(\delta/a) + [\ln(\delta/a)]^2}{0.95425 - \ln(\delta/a)}\right\} \tag{30}$$

where $\Gamma_{1z}$ is the correction to the effective particle friction factor for translation parallel to a single wall. We note that the equivalent equation ob-

tained by Goldman et al. (64) is incorrect, and that their alternative equation, although simpler, is useful only for an extremely limited range of $\delta/a$.

In the limiting case of high gap widths it may be shown that

$$\Gamma_{1z} = \left[1 - \frac{9}{16}\frac{a}{x} + \frac{1}{8}\left(\frac{a}{x}\right)^3 - \frac{45}{256}\left(\frac{a}{x}\right)^4 - \frac{1}{16}\left(\frac{a}{x}\right)^5\right]^{-1} \tag{31}$$

Goldman et al. (64) tabulated calculated values of $\Gamma_{1z}$ for a range of $\delta/a$ from 9.0677 down to 0.0032017. Using tabulations of forces and torques given by O'Neill and coworkers (69, 70), we may obtain values for $\Gamma_{1z}$ for $\delta/a$ down to 0.00045003. A cubic spline fit (e.g., Ref. 71) of all of these $\Gamma_{1z}$ data versus $\ln(\delta/a)$ provides a means of interpolation of accurate $\Gamma_{1z}$. A plot of interpolated $\Gamma_{1z}$ versus $\log_{10}(\delta/a)$ is shown in Fig. 5. The points correspond to the data used to generate the cubic spline fit. Also included are plots of $\Gamma_{1z}$ calculated via the limiting Eqs. (30) and (31). Above the main plot are shown the percentage deviations of these limiting equations



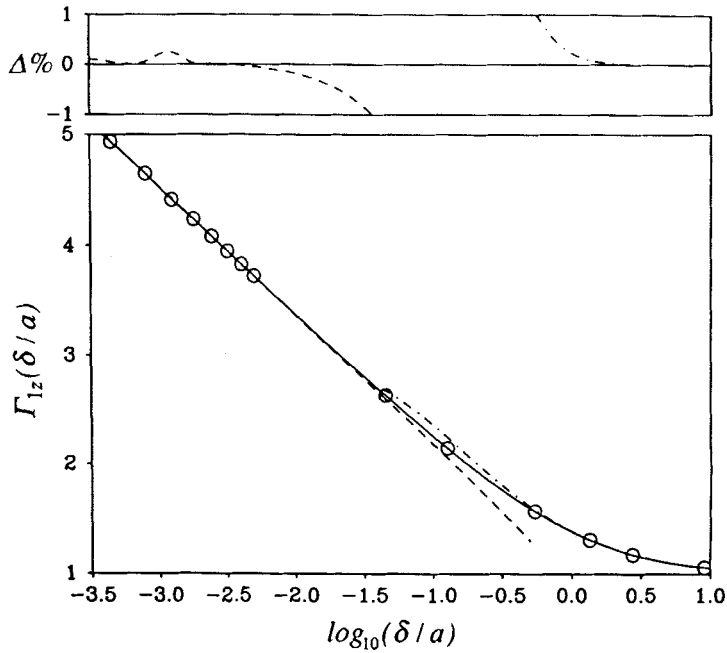


FIG. 5 Plot of the function $\Gamma_{1z}$ obtained by cubic spline interpolation between the points included in the figure. The limiting Eqs. (30) and (31) are also included along with their percentage deviations from interpolation (shown above the main figure).

from interpolated $\Gamma_{1z}$. Equation (30) underestimates $\Gamma_{1z}$ by 1.0, 0.10, and 0.010% at $\delta/a = 0.0365$, 0.00706, and 0.00349, respectively. The apparent oscillation in percent deviation for Eq. (30) at lower $\delta/a$ is likely to be due to small rounding errors in the calculation of $\Gamma_{1z}$ at small $\delta/a$, rather than reflecting some problem with the limiting equation. Equation (31) overestimates $\Gamma_{1z}$ by 1.0, 0.10, and 0.010% at $\delta/a = 0.561$, 1.32, and 2.40, respectively. Accurate values for $\Gamma_{1z}$ may be obtained using Eq. (30) for $\delta/a < 0.00321$ (at this point Eq. 30 and the interpolation intersect), the cubic spline interpolation for $0.00321 \leq \delta/a < 2.40$, and Eq. (31) for $2.40 \leq \delta/a$.

Experiments (72, 73) have confirmed the magnitude of $\Gamma_{1z}$ for $\delta/a$ greater than about 0.02. For smaller $\delta/a$ the measured $\Gamma_{1z}$ appeared to exhibit a "saturation effect" (72) in that it approached a maximum value somewhat greater than 3.0. The apparent deviation from theory may be attributable to particle surface roughness, difficulty in measuring small $\delta$ accurately, or deviation of the wall from a perfect vertical position (73).

As in the case of $\Gamma_x$, when a small particle is close to one of the walls of a parallel plate system the correction to friction factor is likely to be dominated by the presence of the nearer wall and influenced only to a small extent by the further wall. A first-order estimate for $\Gamma_z$, the correction to friction factor for a parallel plate system, may therefore be written as

$$\Gamma_z\left(\frac{x}{a}, \frac{w-x}{a}\right) \approx \Gamma_{1z}\left(\frac{x}{a}\right) + \Gamma_{1z}\left(\frac{w-x}{a}\right) - 1 \tag{32}$$

The force and torque on a particle held in sheared flow near a single plane wall were determined by Goldman, Cox, and Brenner (74). The assumption of zero net force and torque on a freely rotating, neutrally buoyant particle then allowed them to determine the velocity and rate of rotation of a particle entrained in Couette flow near a single wall. Particles were predicted to be retarded relative to the undisturbed fluid streamlines corresponding to the positions of their centers, with the degree of retardation being greater for particles closer to the wall.

In the region close to a wall bounding plane Poiseuille flow, the shear rate is nearly constant. The velocity correction derived for Couette flow may therefore be applied in this region. This approach was taken for the purpose of data reduction in the study of near-wall lift forces using steric field-flow fractionation (45). It was assumed that when no net force acts along the $z$ coordinate, the ratio of particle velocity in the direction of flow to the local fluid velocity was equal to a correction factor $f_1$ which was a function of $\delta/a$. We include the subscript 1 here to signify the single wall correction. The limiting form of $f_1$ close to the wall is given by

$$f_1 = \frac{2.6493 - 3.7157 \ln(\delta/a)}{1.5905 - 3.1881 \ln(\delta/a) + [\ln(\delta/a)]^2} \tag{33}$$

which for $\delta/a \ll 1$ reduces further to

$$f_1 = [0.6661 - 0.2691 \ln(\delta/a)]^{-1} \tag{34}$$

Note that Eq. (34) corrects the error in the equivalent equation obtained by Goldman et al. (74), as we pointed out in the earlier publication (45). Far from the wall the correction factor follows the limiting equation (74)

$$f_1 = 1 - \frac{5}{16}\left(\frac{a}{x}\right)^3 \tag{35}$$

Once again, a cubic spline fit to tabulated data of Goldman et al. (74) [in the form of $1/f_1$ versus $\ln(\delta/a)$] provides a means of interpolation of values for $f_1$. A plot of interpolated $f_1$ versus $\log_{10}(\delta/a)$ is shown in Fig. 6 together with the values predicted via the limiting Eqs. (33) and (35)



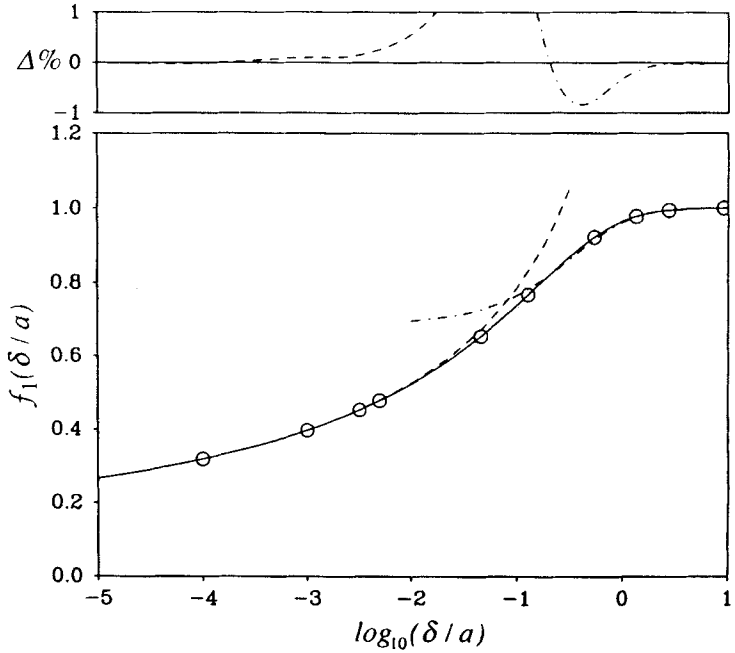


FIG. 6 Plot of the function $f_1$ obtained by cubic spline interpolation between the points included in the figure. The limiting Eqs. (33) and (35) are also included with their percentage deviations from the interpolation shown above the main figure.

and their percentage deviation from interpolated $f_1$. Equation (33) overestimates interpolated $f_1$ by 1.0% at $\delta/a = 0.0170$, and by 0.10% at $\delta/a = 1.89 \times 10^{-3}$. After intersecting the interpolated $f_1$ curve at $\delta/a = 1.49 \times 10^{-4}$, the percent deviation falls to 0.010% at $\delta/a = 2.54 \times 10^{-5}$. Equation (35) overestimates $f_1$ by 1.0% at $\delta/a = 0.0170$, underestimates the function by 0.10% at $\delta/a = 1.69$, and by 0.010% at $\delta/a = 6.68$. We may obtain acceptably accurate $f_1$ using Eq. (33) for $\delta/a < 1.49 \times 10^{-4}$, cubic spline interpolation for $1.49 \times 10^{-4} \leq \delta/a < 6.68$, and Eq. (35) for $6.68 \leq \delta/a$.

Darabauer and Mason (75) reported experimental confirmation of the function $f_1$ predicted by Goldman et al. (74) for a range of $\delta/a$ down to ~0.01. Experiments at closer positions were beyond the capabilities of the optical measurement of $\delta$.

For a small particle ($a/w \ll 1$) entrained in plane Poiseuille flow, a first-order approximation for $f$, the two-wall velocity correction factor, may be written in the form

$$f\left(\frac{x}{a}, \frac{w-x}{a}\right) \approx \left\{\left[f_1\left(\frac{x}{a}\right)\right]^{-1} + \left[f_1\left(\frac{w-x}{a}\right)\right]^{-1} - 1\right\}^{-1} \tag{36}$$

The migration of a particle parallel to two bounding walls was considered by Ganatos, Pfeffer, and Weinbaum (76). The forces and torques on the particle due to its translation and rotation, and due to both Couette and plane Poiseuille flow, were determined at points across the channel thickness for various ratios of $a/w$. Once again, selected results (obtained numerically) were graphed. Knowledge of these quantities allows determination of particle velocity parallel to the walls for any set of applied conditions. The particle may or may not be neutrally buoyant, and the fluid may or may not be quiescent. If the fluid is not quiescent, the flow may be Couette, Poiseuille, or a combination thereof. Any set of conditions yields particle velocity (and rate of rotation) via a simple solution of two simultaneous equations.

Ganatos, Weinbaum, and Pfeffer (77) defined a function F, equivalent to $1/\Gamma_z$, and a function G describing the ratio of particle velocity to $v_{max}$ for entrainment of neutrally buoyant particles in plane Poiseuille flow. They determined the functions numerically for a set of selected conditions, and graphed the results. Examination of these graphed results shows that for particle sizes up to $a/w = 0.1$, the approximate Eqs. (32) and (36) used for the calculation of $\Gamma_z$ and $f$, respectively, are remarkably good. The function $f$ is seen to be slightly overestimated, and therefore particles tend to be a little more retarded than predicted by Eq. (36). Nevertheless, the error is estimated to be less than 2% for all $a/w \leq 0.1$, at all accessible $x/w$. The good agreement for $f$ obtained via Eq. (36) with the numerically

obtained velocity correction factor for plane Poiseuille flow is fortunate, since the function $f_1$ is applicable to the situation of constant shear flow bounded by a single wall.

The velocity component along the $z$-coordinate for a nonneutrally buoyant particle entrained in vertical plane Poiseuille flow is given by

$$v_{pz} = f \cdot v(x/w) + \frac{F_z}{6\pi\eta a \Gamma_z} \tag{37}$$

where $v(x/w)$ is the local fluid velocity given by Eq. (1), and $F_z$ is the force acting on the particle along the $z$-axis and is given by

$$F_z = \frac{4}{3}\pi a^3 \Delta\rho G_z \tag{38}$$

with $\Delta\rho$ being the excess density of the particles over that of the fluid, and $G_z$ is the acceleration due to gravity along the $z$-axis.



## Determination of Particle Trajectory

Consider a small time interval $\delta t$ given by

$$\delta t = \frac{L}{\langle v \rangle N_t} \tag{39}$$

where $N_t$ is the number of time intervals corresponding to the time of migration along the full length $L$ of the cell at the mean fluid velocity $\langle v \rangle$. The distance migrated in this time interval by a particle in the $x$ direction is given by

$$\delta x = v_{px}\delta t = \frac{F_L + F_x}{6\pi\eta a \Gamma_x} \frac{V^0}{\dot{V} N_t} + \frac{\dot{V}_c w}{\dot{V} N_t} \tag{40}$$

where $F_L$ is the local strength of the lift force given by the sum of the contributions described by Eqs. (5), (11), (13), and (15), $F_x$ is the net local force due to applied transverse fields, and $\Gamma_x$ is the local correction to particle friction factor for migration in the $x$ direction. Some limitations must be placed on $\delta x$ in order to obtain an acceptably accurate trajectory determination. First, the accessible region of the channel, which excludes those regions within one radius of the walls, defines the ultimate extent of migration in the $x$ direction, and a $\delta x$ that steps outside this accessible region must be appropriately curtailed. Second, a $\delta x$ that is found to step beyond a stable equilibrium position (these being easily determined in advance of the trajectory calculations) must be reduced. In addition, a $\delta x$ that is found to exceed some preset fraction of $w$ (e.g., $w/200$) is reduced. This latter condition is most likely to be violated in the case of a large

particle located close to a wall. Also, a $\delta x$ that exceeds some fraction of $a$ (e.g., $a/10$), such as may occur for a small particle adjacent to a wall, is reduced. The latter restraint may be limited to the regions $\delta/a < 2.0$ and $(w - x - a)/a < 2.0$, where variations in $F_{Lw}$, $\Gamma_x$, $\Gamma_z$, and $f$ are relatively rapid. When $\delta x$ is adjusted, then $\delta t$ is simply adjusted in proportion. The distance migrated along the cell length in the same time interval ($\delta t$ given by Eq. 39 or an adjusted $\delta t$) is given by

$$\delta z = v_{pz}\delta t = 6\frac{f}{N_t}\frac{x}{w}\left(1 - \frac{x}{w}\right)L + \frac{2a^2\Delta\rho G_z V^0}{9N_t\eta\Gamma_z\dot{V}} \tag{41}$$

where $f$ is the local correction to particle velocity [$= v_{pz}/v(x/w)$], and $\Gamma_z$ is the local correction to particle friction factor for migration along the $z$-axis.

## COMPUTER PROGRAM

The infinite parallel plate model was assumed. The influence of the channel side walls on the carrier velocity profile, and consequently on particle motion, was therefore ignored. Also ignored were the regions close to flow splitters, if present, where the streamlines deviate from linearity. The deviation referred to accommodates the differing inlet and outlet flows as well as the physical presence of the splitter which generally has a significant thickness. Directly following an inlet splitter the sample particles are assumed to be uniformly distributed across the accessible region of the sample lamina lying between wall A and the ISP. The region within a radius of the wall is always inaccessible to the particle centers, and that within a radius of the ISP is assumed to be initially inaccessible.

The program determines and plots trajectories of a number of representative particles of a given size migrating through a channel whose dimensions and flow regime are fixed. The representative particles are initially evenly spaced across the accessible region near the inlet splitter. However, if the particle diameter is equal to or greater than the sample lamina thickness, then only one trajectory is determined, and this is for a particle initially in contact with the accumulation wall for FFF, or wall A for SF. The method of calculation using Eqs. (40) and (41) has already been described. Lift force contributions described by Eqs. (5), (11), (13), and (15) were all taken into account. The correction factors $\Gamma_x$, $\Gamma_z$, and $f$ were calculated via Eqs. (24), (32), and (36), respectively, the single wall contributions being determined as described in the text.

The program was written in FORTRAN 77. Graphical output was generated using the ⟨PLOT79⟩ FORTRAN graphics library (78).

## EXAMPLES OF TRAJECTORY DETERMINATION

It is not feasible to present here the consequences for every possible combination of externally applied fields (both transverse and longitudinal), flow rates (both channel and cross flow), together with resultant hydrodynamic lift forces. Cross flow may be arranged in the direction of or opposed to the forces resulting from interaction with applied fields. The channel flow and forces due to longitudinally applied fields may also act in the same direction or be opposed. Certain combinations of flows and fields have already proved useful in techniques of particle separation. Many combinations remain to be explored. We shall consider just a few interesting examples to illustrate predicted migration in established techniques.

The conditions assumed for Figs. 7(a) and 7(b) correspond exactly to those of Figs. 3(a) and 3(b), respectively. Channel dimensions of $L$ = 10



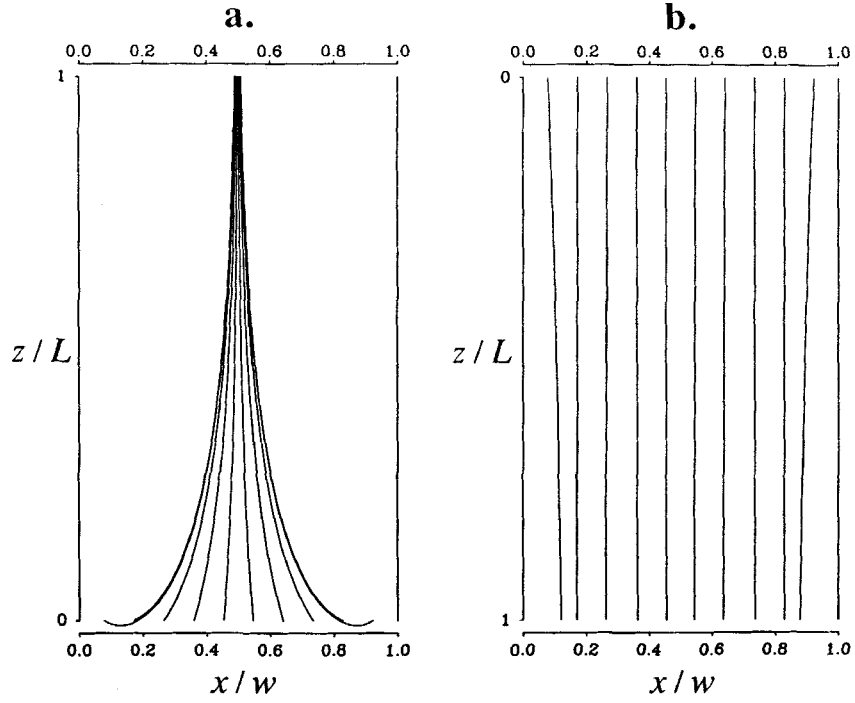


FIG. 7 Set of 10 trajectories for 20 μm diameter copper particles acted upon by the inertial lift forces shown in Fig. 3: (a) upward flow and (b) downward flow. System dimensions: $L$ = 10 cm, $\bar{b}$ = 2 cm, $w$ = 0.033 cm; aqueous carrier flow rate of 1.0 mL/min giving $v_{max}$ = 0.38 cm/s.

cm, $b$ = 2 cm, and $w$ = 0.033 cm were assumed, with a flow rate of aqueous carrier $\dot{V}$ = 1.0 mL/min, this carrier having a density of 0.998 g/mL and a viscosity of 0.00890 poise. Ten trajectories were determined for 20 μm diameter spherical copper particles ($\Delta\rho$ = 7.92 g/mL), initially equally spaced across the accessible thickness of the channel within fully developed upward flow in Fig. 7(a) and downward flow in Fig. 7(b). A near-wall lift force contribution was not included. Such a force has little effect on the systems considered here since the particles are relatively far from the walls. Figure 3(a) shows that for upward flow the net inertial lift force tends to drive the particles away from the walls toward the channel center, and this is borne out by the trajectories shown in Fig. 7(a). It will be noted that the outermost trajectories initially describe a negative migration direction with respect to the $z$-axis. This is because the sedimentation velocity in these parts of the channel exceeds the local fluid velocity. These particles are quickly driven into faster flowing regions however, where they reverse direction. If the particles were not introduced into fully developed flow, as is normally the case, they would tend to sediment out at the bottom of the system. Figure 7(b) shows trajectories of particles that are relatively unaffected by lift forces. Only the outermost trajectories suggest the influence of a net force away from the walls. This is consistent with the variation of net lift force across the channel thickness shown in Fig. 3(b).

Figure 8(a) shows a set of 10 trajectories determined for 20 μm diameter polystyrene beads ($\Delta\rho$ = 0.052 g/mL) introduced into a system having the same dimensions as that considered for Fig. 7. An aqueous flow rate $\dot{V}$ of 1.7 mL/min, with $\dot{V}(a')$ of 0.85 mL/min and a transverse field of 1 gravity were assumed. The broken horizontal line shows the position of the inlet splitting plane at $x/w$ = 0.5. A near-wall lift force with $C$ = 0.10 was included in the calculations. Particles following the lowest three trajectories are found to have sufficient time to reach a stable equilibrium height above wall B before they elute. Figure 8(b) shows the situation predicted for 20 μm diameter neutrally buoyant particles where the influence of a field of 1 gravity is replaced with a downwards cross flow of 1.53 mL/min. This results in a cross flow velocity equal to the Stokes' velocity for the polystyrene particles under 1 gravity. The migration across the channel thickness with cross flow is seen to be faster. This is because particle motion due to entrainment in the cross flow is not impeded by the factor $\Gamma_x$. The critical particle radius as defined by Eq. (29) is calculated to be 30.8 μm, which is far larger than the particles considered. Any particle that has sufficient time to migrate as far as the lower wall is therefore driven into contact, and is predicted to remain at this point of contact and not elute further.

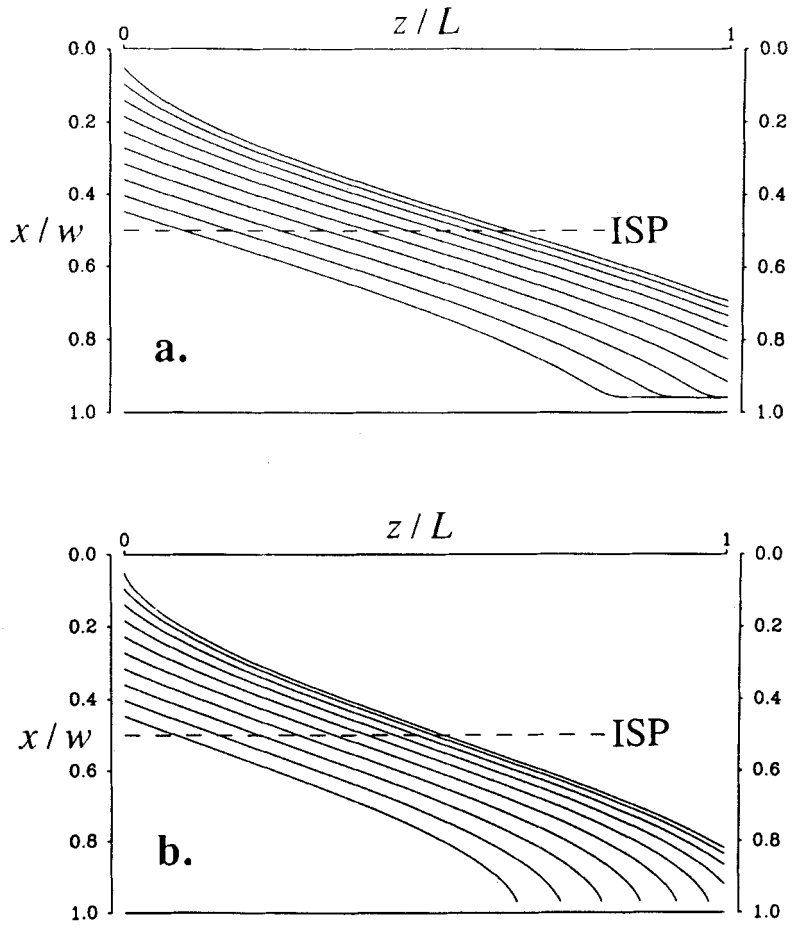


FIG. 8 Set of 10 trajectories for 20 μm particles within a system of the same dimensions as considered for Fig. 7. Aqueous carrier flow rate $\dot{V}$ = 1.7 mL/min with $\dot{V}(a')$ = 0.85 mL/min. Near-wall lift coefficient $C$ = 0.10. Horizontal broken line indicates position of inlet splitting plane (ISP). (a) Polystyrene (PS) particles ($\Delta\rho$ = 0.052 g/mL) with transverse field of 1 gravity. (b) Neutrally buoyant particles with crossflow rate $\dot{V}_c$ = 1.53 mL/min.

Figure 9 illustrates the secondary relaxation of particles toward their respective equilibrium heights following stopped flow primary relaxation in steric FFF. Channel dimensions of $L$ = 90 cm, $\bar{b}$ = 2 cm, and $w$ = 0.0127 cm were assumed. A channel flow rate of 3.05 mL/min, giving $\langle v \rangle$ = 2.0 cm/s, and a field strength of 3 gravities were considered, with five polystyrene particle sizes of 2, 5, 10, 15, and 20 μm diameter. A near-wall lift force was included in the calculations with $C$ = 0.075. The particle

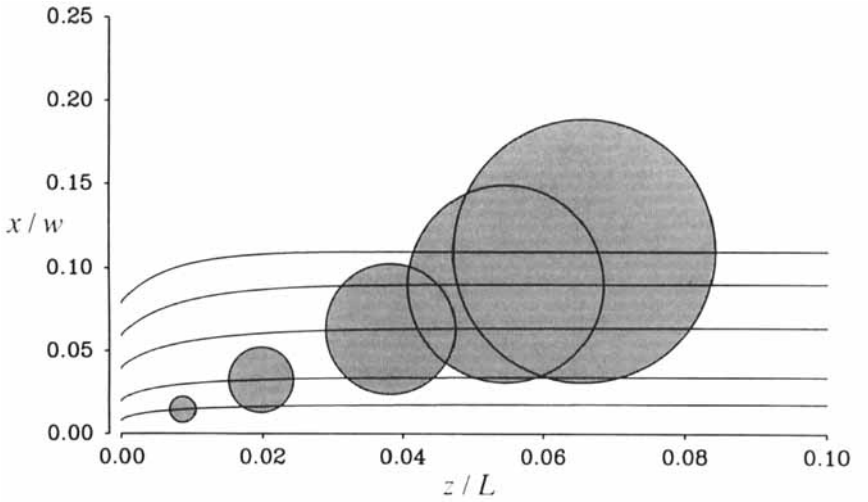


FIG. 9 Trajectories for 2, 5, 10, 15, and 20 μm diameter PS particles following stopped flow relaxation in steric FFF. System dimensions: $L$ = 90 cm, $b$ = 2 cm, $w$ = 0.0127 cm. Aqueous carrier flow rate of 3.05 mL/min ($\langle v \rangle$ = 2.0 cm/s) and field strength of 3 gravities. Near-wall lift coefficient $C$ = 0.075. Particles drawn at 6 seconds after resumption of flow.

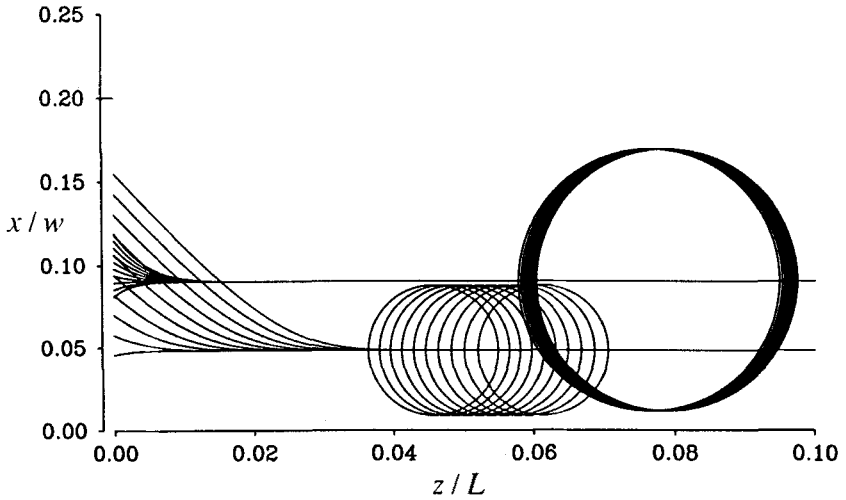


FIG. 10 Sets of 10 trajectories for hydrodynamic relaxation of 10 and 20 μm diameter PS particles in steric FFF. Channel dimensions the same as considered for Fig. 9. $\dot{V}$ = 3.05 mL/min and $\dot{V}_s$ = 0.317 mL/min placing ISP at $x/w$ = 0.20. Field strength of 5 gravities and $C$ = 0.075. Particles drawn at 9 seconds from introduction.

outlines correspond to their predicted positions 6 seconds after the resumption of flow. All particles are seen to quickly reach their equilibrium heights even under these low field conditions.

Finally, Fig. 10 illustrates hydrodynamic relaxation in steric FFF. Channel dimensions correspond to those considered for Fig. 9. The same near-wall lift contribution and channel flow rate were assumed. A $\dot{V}_s$ of 0.317 mL/min, resulting in an inlet splitting plane at $x/w = 0.20$, was also assumed. Sets of 10 trajectories are shown for 10 and 20 μm diameter polystyrene particles migrating under the influence of a transverse field strength of 5 gravities. The particle outlines correspond to their predicted positions 9 seconds after their introduction. At the point of introduction the larger particles are sterically confined to a narrower region at the channel inlet than are the smaller particles. Their starting velocities are therefore more closely similar, and they experience less differential longitudinal displacement during relaxation. The relaxation process is therefore predicted to result in less band spreading in the case of the larger particles. It may also be seen that the two particle sizes are already partially separated from each other after migration along only around 7% of the channel length.



## NOMENCLATURE

| | |
|---|---|
| $a$ | particle radius |
| $a$ | sample inlet adjacent to wall A of SPLITT cell |
| $a'$ | outlet adjacent to wall A of SPLITT cell |
| $a_{crit}$ | critical particle radius given by Eq. (29) |
| A | wall of SPLITT cell at $x = 0$ |
| $b$ | outlet adjacent to wall B of SPLITT cell |
| $b'$ | inlet adjacent to wall B of SPLITT cell |
| $\overline{b}$ | breadth of channel or cell |
| B | wall of SPLITT cell at $x = w$ |
| $C$ | dimensionless coefficient of near-wall lift force Eqs. (14) and (15) |
| $D_T$ | particle thermal diffusion coefficient |
| $e$ | charge on the electron |
| $f$ | correction to particle velocity $[= v_{pz}/v(x/w)]$ along parallel plate system |
| $f_1$ | correction to particle velocity in flow parallel to single plane wall |
| $F_L$ | total lift force |
| $F_{Li}$ | total inertial contribution to lift force |

| | |
|---|---|
| $F_{Li}(I)$ | inertial lift force contribution described by Eq. (5) |
| $F_{Li}(II)$ | inertial lift force contribution described by Eq. (11) |
| $F_{Li}(III)$ | inertial lift force contribution described by Eq. (13) |
| $F_{Lw}$ | near-wall lift force described by Eqs. (14) and (15) |
| $F_x$ | force on particle in $x$ direction due to applied field |
| $F_z$ | force on particle in $z$ direction due to external field |
| $g(x/w)$ | function of $x/w$ included in Eq. (5) |
| $G$ | acceleration due to gravity |
| $G_x$ | component of acceleration along $x$ axis |
| $G_z$ | component of acceleration along $z$ axis |
| $L$ | length of channel or cell |
| $n$ | index of summation in Eq. (19) |
| $N_t$ | number of time intervals corresponding to $L/\langle v \rangle$ |
| Re | channel Reynolds number ($= w v_{max} \rho/\eta$) |
| $s_0$ | fluid shear rate at the wall |
| $T$ | temperature |
| $U_z$ | particle sedimentation velocity in $z$ direction for unbounded fluid |
| $v(x/w)$ | fluid velocity profile across thickness of channel or cell |
| $v_{max}$ | maximum fluid velocity found at $x/w = 0.5$ |
| $v_{px}$ | particle velocity in $x$ direction |
| $v_{pz}$ | particle velocity in $z$ direction |
| $\langle v \rangle$ | mean fluid velocity |
| $V$ | electrical potential |
| $V^0$ | channel or cell void volume |
| $\dot{V}$ | total volumetric flow rate through channel or cell |
| $\dot{V}(a)$ | volumetric flow rate at outlet $a$ of SPLITT cell |
| $\dot{V}(a')$ | volumetric flow rate at sample inlet $a'$ of SPLITT cell |
| $\dot{V}(b)$ | volumetric flow rate at outlet $b$ of SPLITT cell |
| $\dot{V}(b')$ | volumetric flow rate at inlet $b'$ of SPLITT cell |
| $\dot{V}_c$ | volumetric crossflow rate |
| $\dot{V}_f$ | supplementary volumetric carrier flow rate at frit or split inlet of FFF channel |
| $\dot{V}_s$ | volumetric sample flow rate for frit or split inlet FFF channel |
| $w$ | thickness of channel or cell |
| $w_a$ | distance from wall A to outlet splitting plane of SPLITT cell |
| $w_{a'}$ | distance from wall A to inlet splitting plane of SPLITT cell |
| $x$ | distance measured across thickness of FFF channel or SPLITT cell, with origin at accumulation wall of the former and wall A of the latter |

$z$ distance measured from inlet or inlet splitter along length of system

$z$ effective charge on particle

### Greek

$\alpha$ function of $x/w$ defined by Eq. (20)

$\Gamma_x$ correction to particle friction factor for movement along $x$-coordinate of parallel plate system

$\Gamma_{1x}$ correction to particle friction factor for movement perpendicular to single plane wall

$\Gamma_z$ correction to particle friction factor for movement along $z$-coordinate of parallel plate system

$\Gamma_{1z}$ correction to particle friction factor for movement parallel to single plane wall

$\delta$ distance between particle surface and plane wall

$\delta t$ small time interval defined by Eq. (39)

$\delta x$ distance moved by particle in $x$ direction in time $\delta t$

$\delta z$ distance moved by particle in $z$ direction in time $\delta t$

$\Delta\rho$ excess density of particle over that of the fluid

$\eta$ fluid viscosity

$\theta$ intermediate value appearing in Eqs. (2) and (3)

$\rho$ fluid density

$\rho_s$ particle density



## ACKNOWLEDGMENT

This work was supported by Grant CHE-9102321 from the National Science Foundation.

## REFERENCES

1. J. C. Giddings, *Anal. Chem.*, *53*, 1170A–1175A (1981).
2. J. C. Giddings, *Sep. Sci. Technol.*, *20*, 749–768 (1985).
3. J. C. Giddings, *Ibid.*, *21*, 831–843 (1986).
4. M. Martin and P. S. Williams, in *Theoretical Advancement in Chromatography and Related Separation Techniques* (F. Dondi and G. Guiochon, Eds.), (NATO ASI Series C: Mathematical and Physical Sciences, Vol. 383), Kluwer Academic Publishers, Dordrecht, The Netherlands, 1992, pp. 513–580.
5. J. C. Giddings and M. N. Myers, *Sep. Sci. Technol.*, *13*, 637–645 (1978).
6. T. Koch and J. C. Giddings, *Anal. Chem.*, *58*, 994–997 (1986).
7. J. C. Giddings, X. Chen, K.-G. Wahlund, and M. N. Myers, *Ibid.*, *59*, 1957–1963 (1987).
8. S. K. Ratanathanawongs and J. C. Giddings, *J. Chromatogr.*, *467*, 341–356 (1989).

9. P. S. Williams, S. Levin, T. Lenczycki, and J. C. Giddings, *Ind. Eng. Chem. Res.*, *31*, 2172–2181 (1992).
10. C. B. Fuh, S. Levin, and J. C. Giddings, *Anal. Biochem.*, *208*, 80–87 (1993).
11. M. E. Hovingh, G. E. Thompson, and J. C. Giddings, *Anal. Chem.*, *42*, 195–203 (1970).
12. F. J. Yang, M. N. Myers, and J. C. Giddings, *Ibid.*, *49*, 659–662 (1977).
13. J. J. Kirkland, W. W. Yau, W. A. Doerner, and J. W. Grant, *Ibid.*, *52*, 1944–1954 (1980).
14. J. Janča, J. Chmelík, and D. Pribylová, *J. Liq. Chromatogr.*, *8*, 2343–2368 (1985).
15. J. C. Giddings, *Anal. Chem.*, *57*, 945–947 (1985).
16. S. Lee, M. N. Myers, and J. C. Giddings, *Ibid.*, *61*, 2439–2444 (1989).
17. J. C. Giddings, *Ibid.*, *62*, 2306–2312 (1990).
18. M.-K. Liu, P. S. Williams, M. N. Myers, and J. C. Giddings, *Ibid.*, *63*, 2115–2122 (1991).
19. J. C. Giddings, *Sep. Sci. Technol.*, *23*, 931–943 (1988).
20. Y. Gao, M. N. Myers, B. N. Barman, and J. C. Giddings, *Part. Sci. Technol.*, *9*, 105–118 (1991).
21. J. C. Giddings, *Sep. Sci. Technol.*, *23*, 119–131 (1988).
22. J. Zhang, P. S. Williams, M. N. Myers, and J. C. Giddings, In Preparation.
23. J. C. Giddings, M. N. Myers, K. D. Caldwell, and J. W. Pav, *J. Chromatogr.*, *185*, 261–271 (1979).
24. G. Liu and J. C. Giddings, *Anal. Chem.*, *63*, 296–299 (1991).
25. G. Liu and J. C. Giddings, *Chromatographia*, *34*, 483–492 (1992).
26. J. C. Giddings, G. C. Lin, and M. N. Myers, *Sep. Sci.*, *11*, 553–568 (1976).
27. S. R. Springston, M. N. Myers, and J. C. Giddings, *Anal. Chem.*, *59*, 344–350 (1987).
28. C. B. Fuh, M. N. Myers, and J. C. Giddings, *Ind. Eng. Chem Res.*, In Press.
29. S. Levin, M. N. Myers, and J. C. Giddings, *Sep. Sci. Technol.*, *24*, 1245–1259 (1989).
30. S. K. Ratanathanawongs and J. C. Giddings, in *Particle Size Distribution II: Assessment and Characterization* (T. Provder, Ed.), (ACS Symposium Series 472), American Chemical Society, Washington, D.C., 1991, Chap. 15, pp. 229–246.
31. M. A. Benincasa and J. C. Giddings, *Anal. Chem.*, *64*, 790–798 (1992).
32. J. Zhang, Field-Flow Fractionation Research Center, Department of Chemistry, University of Utah, Unpublished Work.
33. B. P. Ho and L. G. Leal, *J. Fluid Mech.*, *65*, 365–400 (1974).
34. F. W. Altena, G. Belfort, J. Otis, F. Fiessinger, J. M. Rovel, and J. Nicoletti, *Desalination*, *47*, 221–232 (1983).
35. F. W. Altena and G. Belfort, *Chem. Eng. Sci.*, *39*, 343–355 (1984).
36. G. Belfort and N. Nagata, *Desalination*, *53*, 57–79 (1985).
37. J. R. Otis, F. W. Altena, J. T. Mahar, and G. Belfort, *Exp. Fluids*, *4*, 1–10 (1986).
38. C. Kleinstreuer and T. P. Chin, *Chem. Eng. Commun.*, *28*, 193–211 (1984).
39. R. G. Cox and H. Brenner, *Chem. Eng. Sci.*, *23*, 147–173 (1968).
40. P. Vasseur and R. G. Cox, *J. Fluid Mech.*, *78*, 385–413 (1976).
41. R. G. Cox and S. K. Hsu, *Int. J. Multiphase Flow*, *3*, 201–222 (1977).
42. J. Otis, Masters Thesis, Rensselaer Polytechnic Institute, Troy, New York, 1983.
43. J. A. Schonberg and E. J. Hinch, *J. Fluid Mech.*, *203*, 517–524 (1989).
44. P. Vasseur and R. G. Cox, *Ibid.*, *80*, 561–591 (1977).
45. P. S. Williams, T. Koch, and J. C. Giddings, *Chem. Eng. Commun.*, *111*, 121–147 (1992).
46. M. H. Moon, Field-Flow Fractionation Research Center, Department of Chemistry, University of Utah, Unpublished Work.
47. P. S. Williams, S. H. Lee, and J. C. Giddings, *Chem. Eng. Commun.*, Submitted.

48. A. D. Maude, *Br. J. Appl. Phys.*, *12*, 293–295 (1961).
49. H. Brenner, *Chem. Eng. Sci.*, *16*, 242–251 (1961).
50. R. G. Cox and H. Brenner, *Ibid.*, *22*, 1753–1777 (1967).
51. F. Durst and H. Raszillier, *Ibid.*, *44*, 2871–2879 (1989).
52. G. D. M. MacKay and S. G. Mason, *J. Colloid Sci.*, *16*, 632–635 (1961).
53. G. D. M. MacKay, M. Suzuki, and S. G. Mason, *Ibid.*, *18*, 103–104 (1963).
54. S. Yuu and Y. Fukui, *AIChE J.*, *27*, 168–170 (1981).
55. A. Ambari, B. Gauthier-Manuel, and E. Guyon, *J. Fluid Mech.*, *149*, 235–253 (1984).
56. G. D. M. MacKay, Ph.D. Thesis, McGill University, Montreal, Canada, 1962.
57. M. D. A. Cooley and M. E. O'Neill, *Mathematika*, *16*, 37–49 (1969).
58. H. A. Lorentz, in *Abhandlungen über Theoretisch Physik. Vol. I*, Druck und Verlag von B. G. Teubner, Leipzig, 1907, Paper II, pp. 23–42. [Initially published in *Amsterdam, Zittingsverlag Akad. v. Wet.*, *5*, 168 (1896).]
59. P. Ganatos, S. Weinbaum, and R. Pfeffer, *J. Fluid Mech.*, *99*, 739–753 (1980).
60. G. S. Beavers and D. D. Joseph, *Ibid.*, *30*, 197–207 (1967).
61. R. Singh and R. L. Laurence, *Int. J. Heat Mass Transfer*, *22*, 721–729 (1979).
62. A. C. Payatakes and G. Dassios, *Chem. Eng. Commun.*, *58*, 119–138 (1987).
63. D. A. Drew, J. A. Schonberg, and G. Belfort, *Chem. Eng. Sci.*, *46*, 3219–3224 (1991).
64. A. J. Goldman, R. G. Cox, and H. Brenner, *Ibid.*, *22*, 637–651 (1967).
65. W. R. Dean and M. E. O'Neill, *Mathematika*, *10*, 13–24 (1963).
66. M. E. O'Neill, *Ibid.*, *11*, 67–74 (1964).
67. H. Faxén, *Ark. Mat. Astrom. Fys.*, *17*(27), 1–28 (1922–23).
68. A. D. Maude, *Br. J. Appl. Phys.*, *14*, 894–898 (1963).
69. M. E. O'Neill and K. Stewartson, *J. Fluid Mech.*, *27*, 705–724 (1967).
70. M. D. A. Cooley and M. E. O'Neill, *J. Inst. Math. Its Appl.*, *4*, 163–173 (1968).
71. W. H. Press, B. P. Flannery, S. A. Teukolsky, and W. T. Vetterling, *Numerical Recipes. The Art of Scientific Computing* (FORTRAN Edition), Cambridge University Press, 1986, pp. 86–89.
72. A. Ambari, B. Gauthier Manuel, and E. Guyon, *J. Phys. Lett.*, *44*, L143–L146 (1983).
73. K. Malysa and T. G. M. van de Ven, *Int. J. Multiphase Flow*, *12*, 459–468 (1986).
74. A. J. Goldman, R. G. Cox, and H. Brenner, *Chem. Eng. Sci.*, *22*, 653–660 (1967).
75. C. L. Darabaner and S. G. Mason, *Rheol. Acta*, *6*, 273–284 (1967).
76. P. Ganatos, R. Pfeffer, and S. Weinbaum, *J. Fluid Mech.*, *99*, 755–783 (1980).
77. P. Ganatos, S. Weinbaum, and R. Pfeffer, *Ibid.*, *124*, 27–43 (1982).
78. This is a collection of FORTRAN subroutines for the generation of graphical output authored by H. V. Mcintosh, Centro de Calculo "Joel Arriaga," Universidad Autonoma de Puebla, 49 Poniente 1102, Puebla, Puebla, Mexico, and N. H. F. Beebe, College of Science Computer, Department of Physics, University of Utah, Salt Lake City, Utah 84112, USA.

*Received by editor May 1, 1993*